Combining Nitrogen Doping and Vacancies for Tunable Resonant States in Graphite

Demba Demba, Abhishek Karn, Cyril Chacon, Yann Girard, Vincent Repain, Amandine Bellec, Hakim Amara, Philippe Lang, Jérôme Lagoute

Combining nitrogen doping and vacancies for tunable resonant states in graphite

Demba Demba,[+,a] Abhishek Karn,[+,a] Cyril Chacon,[a] Yann Girard,[a] Vincent Repain,[a] Amandine Bellec,[a] Hakim Amara,[a,b] Philippe Lang,[c] Jérôme Lagoute*[a]

We investigate the combination of nitrogen doping and vacancies in highly ordered pyrolytic graphite (HOPG), to engineer defect sites with adjustable electronic properties. We combine scanning tunneling microscopy and spectroscopy and density functional theory calculations to reveal the synergistic effects of nitrogen and vacancies in HOPG. Our findings reveal a remarkable shift of the vacancy-induced resonance peak from an unoccupied state in pristine HOPG to an occupied state in nitrogen-doped HOPG. This shift directly correlates with the shift of the charge neutrality point resulting from the n-doping induced by substitutional nitrogen. These results open new avenues for defect engineering in graphite or graphene and achieving novel functionalities for chemical activity or electronic properties.

Introduction

Graphitic carbon materials such as graphite, graphene and carbon nanotubes, share similar atomic structure of sp^2 hybridized carbon atoms. In all these materials, defect engineering, in particular point defects like vacancies[1–3] and nitrogen doping[4–6] has received a special attention. Through the use of scanning tunneling microscopy (STM) and spectroscopy (STS), the structural and electrical characteristics of vacancies in graphite and graphene produced by ion irradiation have been investigated[2,3]. Theoretically, a single vacancy is predicted to generate a sharp resonance at the charge neutrality point (CNP) in the density of states (DOS) of these materials[7–10]. Experimentally, the spectroscopy of single vacancies may show some deviation from this theoretical expectation due to possible local perturbation in real samples. For example, in neutral graphite, the resonant state of a single vacancy has been observed at the Fermi level[2], while in other cases it was found above the Fermi level due to the perturbation of the electronic states of graphite by defects[11,12]. It has also been observed above the Fermi level in graphene, where the Dirac point was shifted to the unoccupied state region due to substrate-induced hole doping[3,13]. In the case of divacancies, STS studies combined with *ab initio* calculations have revealed the formation of unoccupied resonant states[14]. The formation of a resonant state at the CNP has been proposed as a possible source of magnetism in graphite or graphene due to electron-electron interaction that may split the peak into spin up and spin down states[2,13,15].

Substitutional nitrogen dopants are another kind of point defect in carbon materials. In graphene, the insertion of nitrogen atoms in the carbon lattice leads to n-doping[16–18], which can be used to realize band engineering[19]. Akin to vacancies, substitutional nitrogen induces a resonance in the local density of states (LDOS) but which appears in the unoccupied state region (a few tenths of eV above the Dirac point) and that is broader due to the larger density of states of graphene at that energy[17,20,21]. Remarkably, the same resonant state is present in nitrogen doped graphite[22]. Furthermore, Pyridinc nitrogen — a combination of a N atom and a vacancy — causes a resonance in the occupied state region in both graphene[23] and graphite[22]. This observation led to the proposition that these two types of defects can act as Lewis acid or base as a consequence of the presence of unoccupied or occupied state. Subsequent research revealed that pyridinic nitrogen constitute the active sites of nitrogen-doped graphite for oxygen reduction reaction as a result of the occupied state resonance[24]. These findings point to a novel route of defect engineering in carbon materials that involves the introduction of point defects with a controllable energy resonance that can be tuned between occupied and unoccupied state. Here, we describe an original method that makes it possible to accomplish this objective. We combine nitrogen doping with vacancies to tailor the surface of a highly oriented pyrrolitic graphite (HOPG). We create vacancy-type defects by Ar^+ ion irradiation with unoccupied resonant states, then we use nitrogen doping to shift the resonance to the occupied state region. The defects properties are investigated at the atomic scale by STM/STS and density functional theory (DFT) calculations. The method proposed here is a very flexible process that is expected to enable a precise control over the amount of active sites (vacancy concentration) and the energy of the resonant states (energy shift controlled by the nitrogen concentration). Note that backgate devices may also be envisaged to control the energy position of defect resonances. However our approach allows to introduce doping directly at the material level, providing a versatile platform for various

[a] D. Demba, A. Karn, C. Chacon, Y. Girard, V. Repain, A. Bellec, H. Amara, J. Lagoute*
Université Paris Cité, Laboratoire Matériaux et Phénomènes Quantiques, CNRS, F-75013, Paris, France
E-mail: jerome.lagoute@u-paris.fr

[b] H. Amara
Laboratoire d'Etude des Microstructures, ONERA-CNRS, UMR104, Universit´e Paris-Saclay, BP 72, Châtillon Cedex, 92322, France

[c] P. Lang
Université Paris Cité, ITODYS, CNRS, UMR 7086, 15 rue Jean-Antoine de Baïf, 75205 Paris Cedex 13, France

[+] These authors contributed equally.

applications.

Results and Discussion

Figure 1(a) shows the topography of the HOPG sample after Ar^+ ion irradiation (see experimental details for the sputtering condition). The bright spots in the image correspond to the vacancy-type defects induced by the sputtering (see also high resolution images in Fig. S1). With a sputtering duration of one minute, we found that the concentration of point defects is 0.05 % on average (spanning from 0.04 to 0.07 depending on the area investigated). Those defects can exhibit a two, three, or six-fold symmetry as indicated by labels 4, 2 and 9 respectively. It has to be noticed that the six-fold symmetry defects are rather distinct from the others. Indeed they exhibit a ring-like shape which is in strong contrast to the other defects which are point-like defects with a maximum height in their center. Pairs of vacancies in close vicinity (label 6) were also observed. The variety of the topographical features is indicative that not only single vacancies are formed, but that different structural configurations of vacancies are obtained.

In order to obtain more understanding of the nature and properties of these point defects we conducted local dI/dV spectroscopy, which is presented in Fig. 1(b-e). For the point-like defects (1 to 7) a resonance is observed above the Fermi level, in the positive bias range. Note that when the resonance appears at higher bias, the peak is broader (see *e.g.* defect 3 and 5) because the density of states of HOPG is higher. This is different from the general theoretical expectation that a single vacancy should create a resonance at the neutrality point [7–10], which is here at the Fermi level as indicated by the V-shape spectrum centered at zero volt measured on HOPG away from the defects in Fig. 1(b). It is also worth mentioning that our finding is in line with previous reports of unoccupied states observed on single vacancies in graphite [11,12]. Nevertheless, the presence of such resonant states in the case of vacancies in graphene monolayer is seldomly discussed in the literature. It has to be noted that the peak positions may vary even for comparable vacancy configurations. For instance, the apparently identical 3-fold symmetry configuration labeled as 1,2 and 3 have peaks at 180 mV, 160 mV and 280 mV respectively and 2-fold symmetry configuration labeled as 4 and 5 have peaks at 75 mV and 280 mV respectively. While two vacancies in closed vicinity have peaks at 80 mV and 160 mV. Note also that in some cases, a peak close to the Fermi level can be observed (see supporting information Fig. S2). Beside the point defects discussed above, we also occasionally observe ring-like defects with a 6-fold symmetry (defects 8 and 9) that exhibit a peak in negative bias at -100 mV. These observations suggest that the local environment of the sample has a substantial influence on the electronic spectrum of vacancies, or that vacancies with the same topographical feature may show subtle structural differences. Vacancies in graphene or graphite can adopt many structural configurations depending on atomic reconstructions next to the missing atom site [25,26]. Furthermore, the local environment around a point defect can influence its electronic spectrum due to the existence of long-range interaction between defects in graphene [20].

The key point at this stage, is that the majority of vacancy-type defects produced by the ion irradiation procedure exhibit an unoccupied resonant state above the CNP, at positive bias voltage around 110 mV (more details below).

To gain more insight, we have performed *ab-initio* calculations to investigate the electronic properties of vacancies in a graphene monolayer. First, we consider the case of single vacancies where two structures have been reported [25,27] and presented in Fig. 2a and b: a nonreconstructed vacancy with D_{3h} symmetry, and a reconstructed one with C_s symmetry. For the latter, the vacancy is subject to a Jahn-Teller distortion during relaxation, in which the two atoms close to the defect move toward each other, creating a pentagon-like structure, while the third atom is slightly shifted out of the plane. We have therefore calculated the projected density of states (PDOS) of the first neighbour carbon atoms located around the vacancy (see Fig. 2). As already discussed in the literature, the D_{3h} vacancy exhibits a very sharp peak at the Fermi level [7–10]. Moreover, it can also be noted that the atoms belonging to the sublattice of the vacancy (here C2) do not give a resonant state, unlike the C3 site. In other words, the perturbation of the electronic density is concentrated on the first neighbors and on the sites belonging to the sublattice different from that of the vacancy [10]. We now focus on the C_s configuration. Here again, the same dependence of the resonance on the sublattice observed in the case of D_{3h} configuration is recovered. More interestingly, this structure gives rise to an unoccupied state above the Fermi level (around 0.2 eV) which highlights that the reconstruction of the vacancy involves a shift from the resonant state at the neutrality point to unoccupied states. Furthermore, we have also considered a divacancy since it is also a defect of great interest which is known to be stable through energy gain with respect to two isolated monovacancies in carbon structures [25,28]. This corresponds to a structure where two neighbouring vacancies coalesce during relaxation, resulting in the displacement of the atoms closest to the defect, thereby giving rise to pentagonal structures (see Fig. 2c). In this particular case, there is no significant resonance driven by the sublattices due to the high loss of symmetry caused by this defect. More simply, we clearly see that the amplitude of the resonance decreases as the distance from the vacancy increases. In addition, our DFT calculations show the presence of an unoccupied state in the electronic spectrum. Therefore, our DFT calculations conclusively reveal the reconstructed single vacancies and divacancies as the origin of the unoccupied states experimentally observed. This allows us to identify the point defects obtained by ion irradiation as single or double vacancies.

Next, we consider nitrogen doped HOPG. The substitutional nitrogen atoms appear as bright spots with a triangular symmetry that is due to charge transfers from N atom to local C atoms [16–19,22] (see figure 3(a) and Fig. S3. The dopants appear as individualistic substitutional N, which is the most common configuration.

Similar to graphene, the insertion of nitrogen in the carbon lattice of graphite causes a n-doping. This is revealed by the STS spectrum measured on the HOPG region, away from the nitrogen sites (see the inset of Figure 3 (a)). The dI/dV spectrum exhibits the expected V-shape together with a gap-like feature around the Fermi energy that results from a phonon-mediated inelastic tunneling at $\sim$ 65

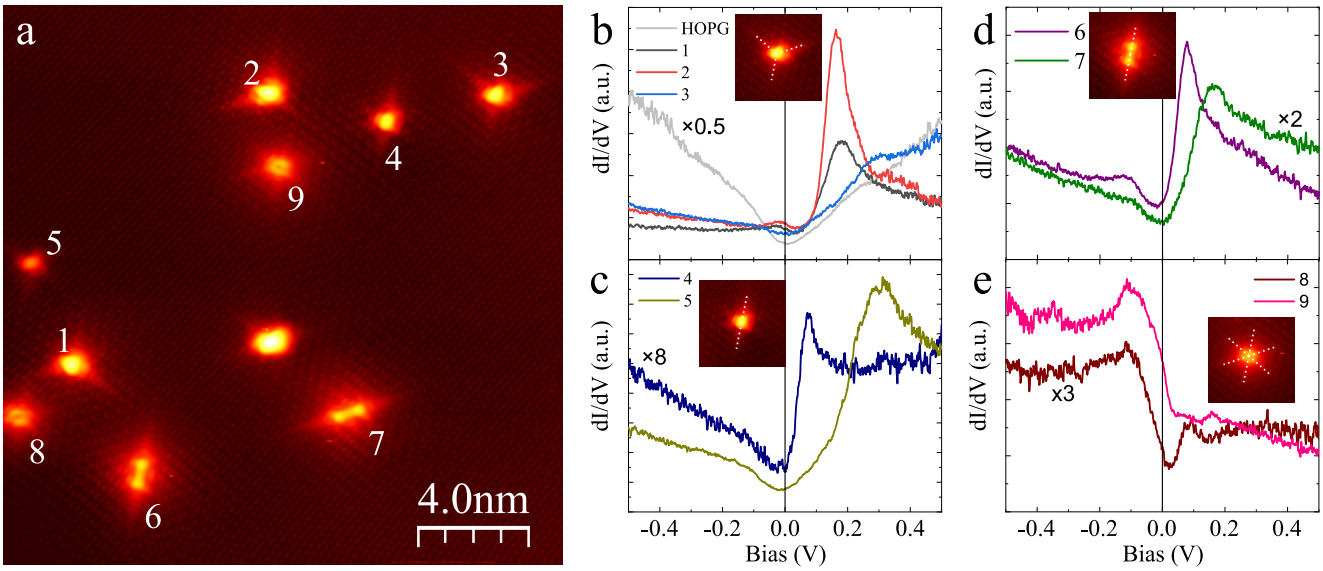

Figure 1. (a) STM image of HOPG after exposition to Ar^+ ion irradiation ($V = 0.2$ V, $I = 200$ pA). (b-e) dI/dV spectra measured on vacancy defects labeled by their respective number in (a). A reference spectrum on HOPG is shown in (a) (grey curve). The Fermi level is indicated by a vertical line in the spectra. Insets in (b-e) are zoom on defects 3, 4, 6 and 9 respectively, with dot lines as guide to the eye highlighting the scattering pattern around the defects.

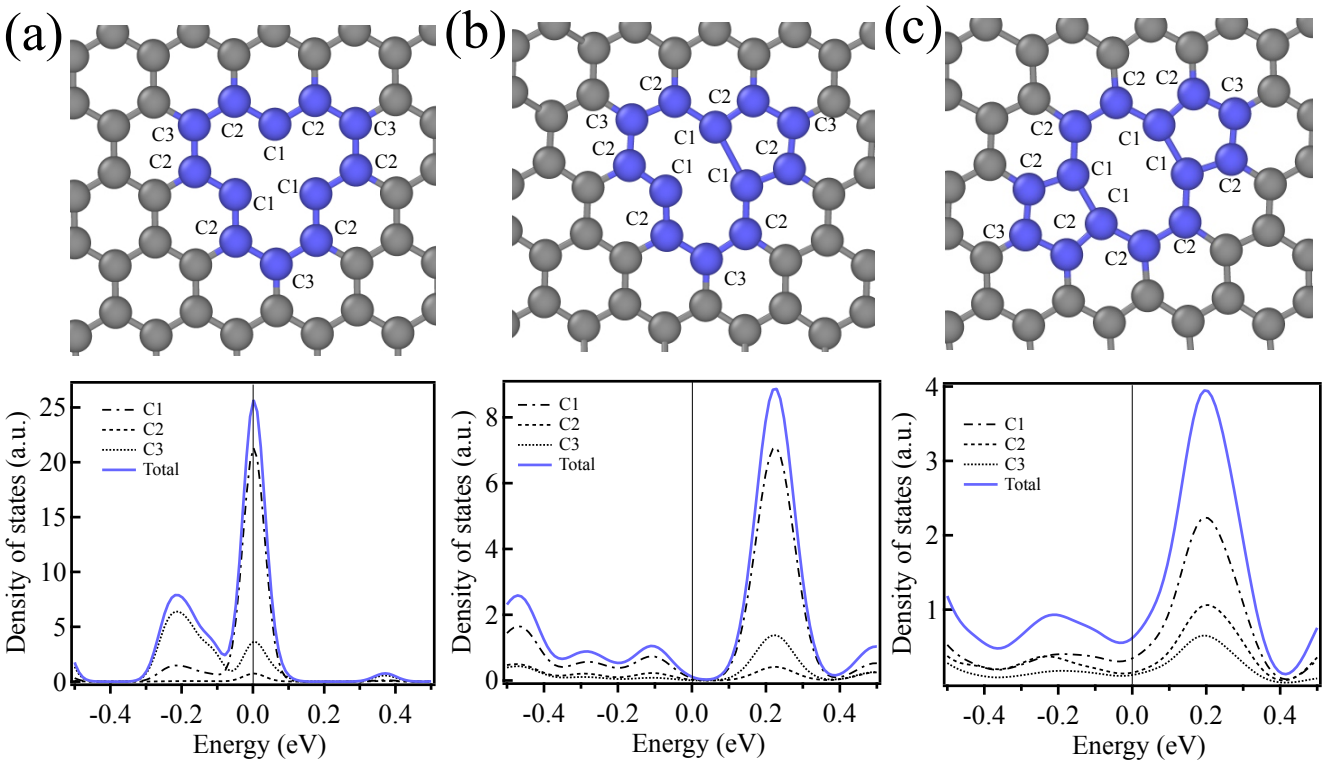

Figure 2. Fully optimized structures of three vacancy type defects and the PDOS of the carbon atoms close to the defect: the first, second, and third neighbors (C1, C2, and C3) coloured in blue as well as their total contribution. The PDOS of C1, C2 C3 are the sum over all atoms in first, second or third neighbor position, respectively. (a) Nonreconstructed vacancy with *D3h* symmetry. (b) Reconstructed vacancy with *Cs* symmetry. (c) Divacancy. The Fermi level is set to zero.

mV[6,29]. Comparatively to undoped HOPG, the CNP is shifted below the Fermi level, and appears as a dip at -0.28 V. This is the fingerprint of the n-doping of HOPG that results from substitutional nitrogen. The doping level depends on the nitrogen doping amount. Therefore, we have estimated the nitrogen concentration in the sample by counting the N dopants in the topographical images and found a concentration of 0.18% N atoms per C atoms. The value of the CNP we obtain is quite similar to what has been obtained in graphene[16,18]. This indicates that the nitrogen electronic doping effect in graphite is comparable to that in graphene. Regarding the electronic structure of N dopants, we mea-

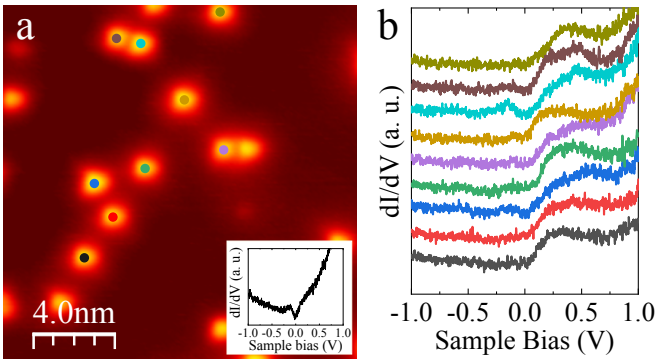

Figure 3. (a) STM image of HOPG after nitrogen doping ($V = 0.5$ V, $I = 50$ pA). The inset shows the dI/dV spectrum measured on HOPG area far from nitrogen sites. (b) dI/dV spectra measured on several nitrogen dopants indicated by dot symbols with corresponding color code.

sured several spectra on different N atoms (see figure 3 (b)). All spectra evidence an asymmetrical DOS spectrum and an empty-state resonance manifested by a broad peak located between 0.3 and 0.5 V. This resonance is typical of a substitutional nitrogen atom and has been observed in graphite and graphene[17,21–23] and discussed theoretically[20].

We turn now to the combination of nitrogen and vacancies in HOPG, which is the main finding of this work. Starting from the nitrogen doped HOPG that we presented above, we exposed the sample to Ar^+ irradiation for 3 minutes in order to create vacancies, targeting a vacancy defects concentration of 0.15 %. Note that we have also tried to create combined defects in opposite way, vacancy first and nitrogen second, but it was unclear whether the vacancies were clearly still present, because nitrogen atoms may have filled some vacancy sites. This specific point needs more work to be clarified. The topography of the HOPG surface exposed to nitrogen plasma source followed by and Ar^+ ion irradiation is shown in Fig. 4a. The total concentration of defects was found to be of 0.3 %, which is close to the sum of nitrogen concentration (0.18 %) and expected vacancies concentration (0.15 %). The majority of point defects can be divided into 2 categories, type I and type II, depending on their topographical signature. At a bias voltage of +0.5 V (Fig. 4a), Type I defects (such as N_1 to N_3) appear brighter and wider than type II defects (1 to 6). This contrast is inverted at -0.5 V (see supporting information Fig. S4), which indicates that the contrast is dominated by electronic effects. To further identify those defects, we carefully acquired the STS spectra on the sample. Figure 4b shows the spectra taken on defect free region that exhibit the expected inelastic phonon excitation feature around the Fermi level and the CNP at -0.3 V. On type I defects, the spectra, which are shown in Fig. 4(c), exhibit a broad resonance at positive bias, similar to nitrogen defects shown in Fig. 3(b). Therefore, we attribute type I defects to substitutional nitrogen. Remarkably, type II defects exhibit a sharp resonance peak below the Fermi level. This explains the voltage dependent topographical contrast observed: at +0.5 V, the nitrogen appears higher because its resonance is integrated in the tunneling current while the vacancies have no state included in this energy range. The opposite happens at negative bias where only vacancies have a peak in their spectrum. The atomic resolution image shown in the inset of Fig.4(a) reveals the expected triangular shape for nitrogen dopants, and a two-fold symmetry for the defect 6. The topography of defect 6 corresponds to the expected image for a divacancy. A histogram plot of resonance peak distribution of type II defects is shown in Fig. 5. The statistics show that the peak is at negative bias and is centered around -170 mV. This value has to be compared with the distribution of resonant state position on undoped HOPG which is centered at 110 mV (Fig. 5). This comparison shows that the vacancy resonant state on N-HOPG is shifted by 280 mV below the position measured on undoped HOPG. This shift is in agreement with the shift of the CNP of the sample that is around 300 mV. All these observations point toward the fact that type II defects correspond to vacancy defects created by the ion irradiation with a resonance that has been shifted below the Fermi level due to the nitrogen doping.

These observations allow us to propose a new route for defect engineering in graphite or graphene by combining nitrogen doping and vacancy. The vacancies create defect sites with a sharp resonance in the density of states, while nitrogen is used to tune the energy position of this resonance. This allows the creation of vacancy-type defects with occupied or non-occupied resonant states as needed. This method is highly versatile. It is a post-synthesis method, which means it can be applied to any sample regardless of its substrate or synthesis route. The concentration of vacancy sites can be fully controlled by adjusting the ion irradiation time, and the energy position of the resonant state can be tuned by controlling the nitrogen concentration. Note that this route provides a means to introduce a controllable quantity of point defects with an occupied resonant state, which is difficult to achieve through other methods.

Conclusion

To summarize, we have tuned the electronic properties of HOPG by combining vacancies and substitutional nitrogen that were produced independently. STM experiments and DFT calculations reveal that single vacancies and divacancies induce a resonance peak above the Fermi level in a neutral HOPG. This state falls below the Fermi level when nitrogen is introduced because it shifts the electronic spectrum of HOPG to a lower energy due to n-doping. This technique provides a way to realize on demand point defects with an occupied or unoccupied localized resonant state. It must be noted that the method presented here is very flexible and versatile. In case of standard nitrogen doping, a change in concentration of vacancies sites contained in pyridinic-N, which are active sites, involves a change in the doping level (due to a change in nitrogen amount). In our strategy, a change in concentration of vacancies sites is totally independent from the doping level. Moreover, we anticipate that the concentration of nitrogen dopants can be used to move the energy position of vacancy electronic state to a desired value. This might lead to new possibilities for defect engineering in HOPG or graphene to realize active sites for chemical, catalytic or electronic functionalities.

Experimental Section

Experimental details The study was performed under ultra high vacuum conditions (UHV) on commercially avail-

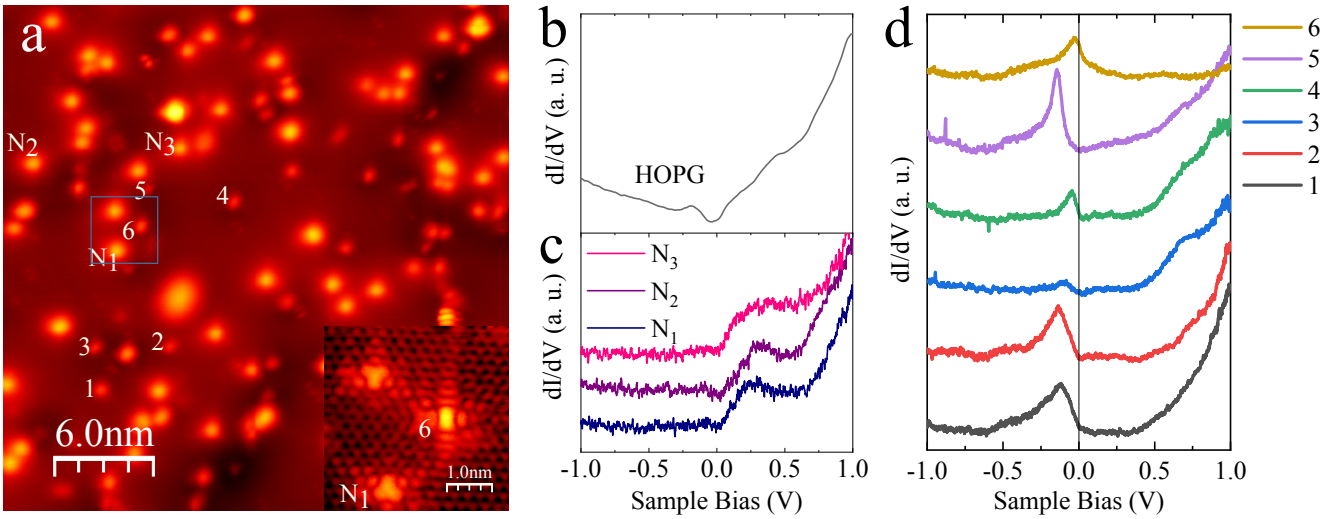

Figure 4. (a) STM image of HOPG after nitrogen doping and Ar^+ ion irradiation ($V = 0.5$ V, $I = 100$ pA). The inset is an atomic resolution image of the area marked by a square in the large scale image. (b) Reference dI/dV spectrum Measured on the sample far from point defects. (c) dI/dV spectra measured on nitrogen dopants. (d) dI/dV spectra measured on vacancy defects.

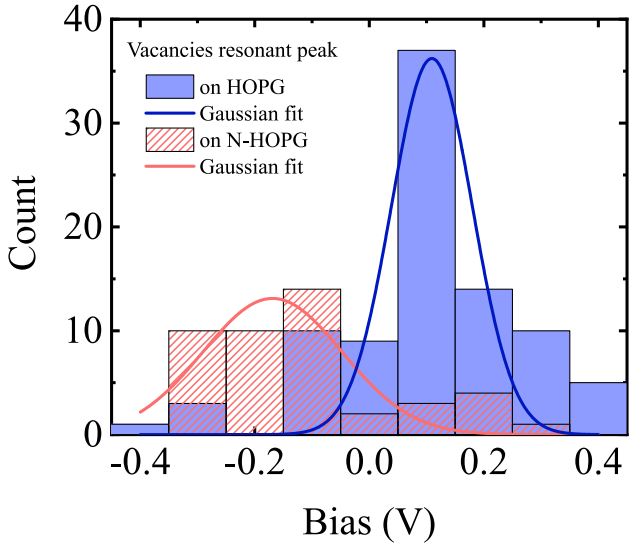

Figure 5. Statistical distribution and gaussian fit of the vacancies peak position on undoped HOPG and on nitrogen doped HOPG.

able HOPG (SP1 grade). HOPG samples were cleaved in air and degassed under UHV at 600°C. Vacancies were obtained by exposing the sample to argon ions produced by a sputtering gun. We used an Ar^+ ions energy of 300 eV by combining an accelerating voltage of 500 V at the ion gun and a bias voltage of 200 V on the sample. The nitrogen-doping was performed by exposing the HOPG sample to a flux of nitrogen radicals produced by a remote radio-frequency plasma source fed with N_2. The pressure in the chamber during doping was 4.10^{-4} mbar, the plasma power was 200 W. After inducing defects, the HOPG samples were degassed again at 600°C. All the STM/STS measurements were performed on a Omicron low temperature STM working at 78 K and a pressure lower than 1×10^{-10} mbar. The STS Spectra were acquired using a lock-in detector at a frequency around 716 Hz and a modulation amplitude of 20 mV approximately. The measurements were performed with an electrochemically etched tungsten tip previously calibrated in a clean Au(111) monocrystal until obtaining satisfying Shockley state at -0.5 V in the Au surface spectra. The clean Au(111) substrate was prepared by standard Ar^+ sputtering and annealing under UHV conditions.

Computational details The electronic properties were investigated using the Quantum Espresso code[30,31], based on density functional theory (DFT) within the local density approximation (LDA). A norm-conserving pseudopotential was used for the carbon atom, and the plane wave basis set was given a cutoff energy 50 Ry for the wavefunctions and of 200 Ry for the charge. The exchange-correlation potential has been approximated with the Perdew-Burke-Ernzerhof model[32]. The system consists of a central defect site within a supercell sufficiently large to minimize boundary effects. We adopted a (10×10) grid of 200 atoms. The size of the supercell in the c direction was set to 10 Åto avoid the interaction between neighboring defects. Integrations over the Brillouin zone are based on a 6×6 Monkhorst-Pack 2D grid[33], which is sufficiently fine to ensure the numerical convergence of all the calculated properties. All the structures were fully relaxed using the Broyden-Fletcher-Goldfarb-Shanno minimization scheme, keeping the supercell geometry fixed. The atomic positions are relaxed until the forces on the atoms are reduced to 10^{-6} hartree/bohr. Last, all the projected density of states (PDOS) presented have been obtained with a peak width of 0.05 eV for broadening the eigenvalues.

Acknowledgements

We thank the French National Research Agency (ANR-20-CE09-0023 DEFINE2D project) for financial support. This project has received financial support from the CNRS through the MITI interdisciplinary programs.

Conflict of Interest

The authors declare no conflict of interest.

Keywords: HOPG • Vacancy • Nitrogen doping • Scanning tunneling microscopy • DFT

References

[1] A. V. Krasheninnikov, F. Banhart, Nat. Mater. **2007**, 6, 723.

[2] M. M. Ugeda, I. Brihuega, F. Guinea, J. M. Gómez-Rodríguez, Phys. Rev. Lett. **2010**, 104, 096804.

[3] M. M. Ugeda, D. Fernández-Torre, I. Brihuega, P. Pou, A. J. Martínez-Galera, R. Pérez, J. M. Gómez-Rodríguez, Phys. Rev. Lett. **2011**, 107, 116803.

[4] P. Ayala, R. Arenal, M. Rümmeli, A. Rubio, T. Pichler, Carbon **2010**, 48, 575.

[5] H. Wang, T. Maiyalagan, X. Wang, Acs Catal. **2012**, 2, 781.

[6] F. Joucken, L. Henrard, J. Lagoute, Phys. Rev. Mater. **2019**, 3, 110301.

[7] T. O. Wehling, A. V. Balatsky, M. I. Katsnelson, A. I. Lichtenstein, K. Scharnberg, R. Wiesendanger, Phys. Rev. B **2007**, 75, 125425.

[8] V. M. Pereira, J. M. B. Lopes dos Santos, A. H. Castro Neto, Phys. Rev. B **2008**, 77, 115109.

[9] W.-M. Huang, J.-M. Tang, H.-H. Lin, Phys. Rev. B **2009**, 80, 121404.

[10] F. Ducastelle, Phys. Rev. B **2013**, 88, 075413.

[11] J. Oh, T. Kondo, D. Hatake, Y. Honma, K. Arakawa, T. Machida, J. Nakamura, J. Phys : Condens Matter **2010**, 22, 304008.

[12] T. Kondo, Y. Honma, J. Oh, T. Machida, J. Nakamura, Phys. Rev. B **2010**, 82, 153414.

[13] Y. Zhang, S.-Y. Li, H. Huang, W.-T. Li, J.-B. Qiao, W.-X. Wang, L.-J. Yin, K.-K. Bai, W. Duan, L. He, Phys. Rev. Lett. **2016**, 117, 166801.

[14] M. M. Ugeda, I. Brihuega, F. Hiebel, P. Mallet, J.-Y. Veuillen, J. M. Gómez-Rodríguez, F. Ynduráin, Phys. Rev. B **2012**, 85, 121402.

[15] H. González-Herrero, J. M. Gómez-Rodríguez, P. Mallet, M. Moaied, J. J. Palacios, C. Salgado, M. M. Ugeda, J.-Y. Veuillen, F. Yndurain, I. Brihuega, Science **2016**, 352, 437.

[16] L. Zhao, R. He, K. T. Rim, T. Schiros, K. S. Kim, H. Zhou, C. Gutierrez, S. P. Chockalingam, C. J. Arguello, L. Palova, D. Nordlund, M. S. Hybertsen, D. R. Reichman, T. F. Heinz, P. Kim, A. Pinczuk, G. W. Flynn, A. N. Pasupathy, Science **2011**, 333, 999.

[17] F. Joucken, Y. Tison, J. Lagoute, J. Dumont, D. Cabosart, B. Zheng, V. Repain, C. Chacon, Y. Girard, A. R. Botello-Méndez, S. Rousset, R. Sporken, J.-C. Charlier, L. Henrard, Phys. Rev. B **2012**, 85, 161408.

[18] F. Joucken, Y. Tison, P. Le Fèvre, A. Tejeda, A. Taleb-Ibrahimi, E. Conrad, V. Repain, C. Chacon, A. Bellec, Y. Girard, S. Rousset, J. Ghijsen, R. Sporken, H. Amara, F. Ducastelle, J. Lagoute, Sci. Rep. **2015**, 5, 14564.

[19] M. Bouatou, C. Chacon, A. B. Lorentzen, H. T. Ngo, Y. Girard, V. Repain, A. Bellec, S. Rousset, M. Brandbyge, Y. J. Dappe, J. Lagoute, Adv. Funct. Mater. **2022**, 32, 2208048.

[20] P. Lambin, H. Amara, F. Ducastelle, L. Henrard, Phys. Rev. B **2012**, 86, 045448.

[21] M. Telychko, K. Noori, H. Biswas, D. Dulal, Z. Chen, P. Lyu, J. Li, H.-Z. Tsai, H. Fang, Z. Qiu, Z. W. Yap, K. Watanabe, T. Taniguchi, J. Wu, K. P. Loh, M. F. Crommie, A. Rodin, J. Lu, Nano Lett. **2022**, 22, 8422.

[22] T. Kondo, S. Casolo, T. Suzuki, T. Shikano, M. Sakurai, Y. Harada, M. Saito, M. Oshima, M. I. Trioni, G. F. Tantardini, J. Nakamura, Phys. Rev. B **2012**, 86, 035436.

[23] Y. Tison, J. Lagoute, V. Repain, C. Chacon, Y. Girard, S. Rousset, F. Joucken, D. Sharma, L. Henrard, H. Amara, A. Ghedjatti, F. Ducastelle, ACS Nano **2015**, 9, 670.

[24] D. Guo, R. Shibuya, C. Akiba, S. Saji, T. Kondo, J. Nakamura, Science **2016**, 351, 361.

[25] H. Amara, S. Latil, V. Meunier, P. Lambin, J.-C. Charlier, Phys. Rev. B **2007**, 76, 115423.

[26] A. W. Robertson, B. Montanari, K. He, C. S. Allen, Y. A. Wu, N. M. Harrison, A. I. Kirkland, J. H. Warner, ACS Nano **2013**, 7, 4495.

[27] A. A. El-Barbary, R. H. Telling, C. P. Ewels, M. I. Heggie, P. R. Briddon, Phys. Rev. B **2003**, 68, 144107.

[28] A. Krasheninnikov, P. Lehtinen, A. Foster, R. Nieminen, Chem. Phys. Lett. **2006**, 418, 132.

[29] Y. Zhang, V. W. Brar, F. Wang, C. Girit, Y. Yayon, M. Panlasigui, A. Zettl, M. F. Crommie, Nat. Phys. **2008**, 4, 627.

[30] P. Giannozzi, S. Baroni, N. Bonini, M. Calandra, R. Car, C. Cavazzoni, D. Ceresoli, G. L. Chiarotti, M. Cococcioni, I. Dabo, A. D. Corso, S. de Gironcoli, S. Fabris, G. Fratesi, R. Gebauer, U. Gerstmann, C. Gougoussis, A. Kokalj, M. Lazzeri, L. Martin-Samos, N. Marzari, F. Mauri, R. Mazzarello, S. Paolini, A. Pasquarello, L. Paulatto, C. Sbraccia, S. Scandolo, G. Sclauzero, A. P. Seitsonen, A. Smogunov, P. Umari, R. M. Wentzcovitch, J. Phys : Condens Matter **2009**, 21, 395502.

[31] P. Giannozzi, O. Andreussi, T. Brumme, O. Bunau, M. B. Nardelli, M. Calandra, R. Car, C. Cavazzoni, D. Ceresoli, M. Cococcioni, N. Colonna, I. Carnimeo, A. D. Corso, S. de Gironcoli, P. Delugas, R. A. DiStasio, A. Ferretti, A. Floris, G. Fratesi, G. Fugallo, R. Gebauer, U. Gerstmann, F. Giustino, T. Gorni, J. Jia, M. Kawamura, H.-Y. Ko, A. Kokalj, E. Küçükbenli, M. Lazzeri, M. Marsili, N. Marzari, F. Mauri, N. L. Nguyen, H.-V. Nguyen, A. O. de-la Roza, L. Paulatto, S. Poncé, D. Rocca, R. Sabatini, B. Santra, M. Schlipf, A. P. Seitsonen, A. Smogunov, I. Timrov, T. Thonhauser, P. Umari, N. Vast, X. Wu, S. Baroni, J. Phys : Condens Matter **2017**, 29, 465901.

[32] J. P. Perdew, K. Burke, M. Ernzerhof, Phys. Rev. Lett. **1996**, 77, 3865.

[33] J. D. Pack, H. J. Monkhorst, Phys. Rev. B **1977**, 16, 1748.

Entry for the Table of Contents

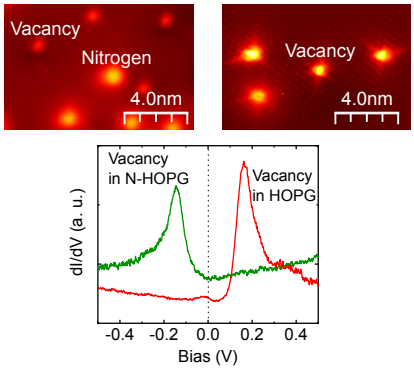

Vacancies in graphite are characterised by an unoccupied resonant peak above the Fermi level. Upon nitrogen doping, this peak is downshifted below the Fermi level and becomes occupied. This specific combination of defects unlocks exciting possibilities for tailoring the properties of advanced materials through a synergistic approach.